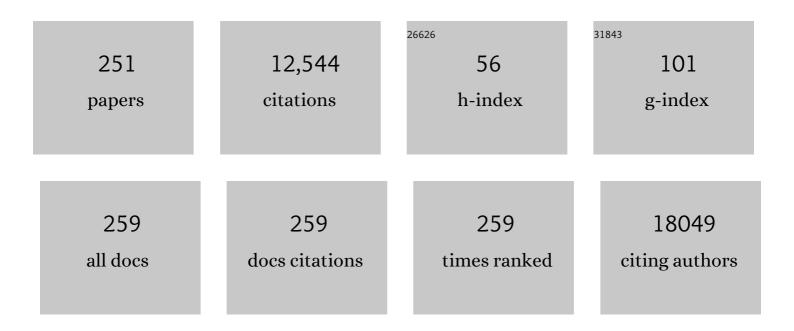
## Jonas Baltrusaitis

List of Publications by Year in descending order

Source: https://exaly.com/author-pdf/303702/publications.pdf Version: 2024-02-01



#	Article	IF	CITATIONS
1	Molecular structure and catalytic promotional effect of Mn on supported Na2WO4/SiO2 catalysts for oxidative coupling of methane (OCM) reaction. Catalysis Today, 2023, 416, 113837.	4.4	10
2	Elucidating the underlying surface chemistry of Sn/Al2O3 catalysts during the propane dehydrogenation in the presence of H2S co-feed. Applied Surface Science, 2022, 573, 151205.	6.1	7
3	Definition of a new (Doniachâ€Sunjicâ€Shirley) peak shape for fitting asymmetric signals applied to reduced graphene oxide/graphene oxide XPS spectra. Surface and Interface Analysis, 2022, 54, 67-77.	1.8	25
4	Catalytic reduction of 4-nitrophenol using CuO@Na <sub>2</sub> Ti(PO <sub>4</sub> ) <sub>2</sub> â <h<sub>2O. Journal of Environmental Science and Health - Part A Toxic/Hazardous Substances and Environmental Engineering, 2022, 57, 65-79.</h<sub>	1.7	3
5	Heterogeneous photo-Fenton-like degradation of emerging pharmaceutical contaminants in wastewater using Cu-doped MgO nanoparticles. Applied Catalysis A: General, 2022, 630, 118468.	4.3	13
6	The Effect of Pelletized Lime Kiln Dust Combined with Biomass Combustion Ash on Soil Properties and Plant Yield in a Three-Year Field Study. Land, 2022, 11, 521.	2.9	2
7	Scale-Up of Agrochemical Urea-Gypsum Cocrystal Synthesis Using Thermally Controlled Mechanochemistry. ACS Sustainable Chemistry and Engineering, 2022, 10, 6743-6754.	6.7	21
8	CO2 conversion to syngas via electrification of endothermal reactors: Process design and environmental impact analysis. Energy Conversion and Management, 2022, 265, 115763.	9.2	7
9	A study of in situ reduction of MoO3 to MoO2 by X-ray Photoelectron Spectroscopy. Applied Surface Science, 2022, 598, 153827.	6.1	22
10	Characterization and Toxicity Analysis of Lab-Created Respirable Coal Mine Dust from the Appalachians and Rocky Mountains Regions. Minerals (Basel, Switzerland), 2022, 12, 898.	2.0	5
11	Role and Responsibility of Sustainable Chemistry and Engineering in Providing Safe and Sufficient Nitrogen Fertilizer Supply at Turbulent Times. ACS Sustainable Chemistry and Engineering, 2022, 10, 8997-9001.	6.7	22
12	Extraction of selected rare earth elements from anthracite acid mine drainage using supercritical CO2 via coagulation and complexation. Journal of Rare Earths, 2021, 39, 83-89.	4.8	14
13	Immobilization and activation of cobalt-amine catalyst on NH4OH-treated activated carbon for ethylene dimerization. Catalysis Today, 2021, 365, 24-34.	4.4	4
14	Physicochemical Characterization of Pelletized Lime Kiln Dust as Potential Liming Material for Acidic Soils. Waste and Biomass Valorization, 2021, 12, 1267-1280.	3.4	8
15	Nutrient Dynamics and Plant Response in Soil to Organic Chicken Manure-Based Fertilizers. Waste and Biomass Valorization, 2021, 12, 371-382.	3.4	10
16	Optimization of energy requirements for CO2 post-combustion capture process through advanced thermal integration. Fuel, 2021, 283, 118940.	6.4	42
17	Dynamic simulation and control of a combustion turbine process for biogas derived methane. Computers and Chemical Engineering, 2021, 144, 107121.	3.8	6
18	Unraveling spectral shapes of adventitious carbon on gold using a time-resolved high-resolution X-ray photoelectron spectroscopy and principal component analysis. Applied Surface Science, 2021, 538, 148031.	6.1	10

#	Article	IF	CITATIONS
19	Oxidative Dehydrogenation of Propane to Propylene with Soft Oxidants via Heterogeneous Catalysis. ACS Catalysis, 2021, 11, 2182-2234.	11.2	97
20	A Spectroscopic Study of Supportedâ€Phosphateâ€Catalysts (SPCs): Evidence of Surfaceâ€mediated Hydrogenâ€Transfer. ChemCatChem, 2021, 13, 2064-2073.	3.7	5
21	Elucidating the origin of selective dehydrogenation of propane on Î <sup>3</sup> -alumina under H2S treatment and co-feed. Journal of Catalysis, 2021, 394, 142-156.	6.2	21
22	A Mixture of Green Waste Compost and Biomass Combustion Ash for Recycled Nutrient Delivery to Soil. Agronomy, 2021, 11, 641.	3.0	3
23	Elucidating the Effects of Mn Promotion on SiO <sub>2</sub> -Supported Na-Promoted Tungsten Oxide Catalysts for Oxidative Coupling of Methane (OCM). ACS Catalysis, 2021, 11, 10131-10137.	11.2	23
24	New Mechanistic and Reaction Pathway Insights for Oxidative Coupling of Methane (OCM) over Supported Na <sub>2</sub> WO <sub>4</sub> /SiO <sub>2</sub> Catalysts. Angewandte Chemie - International Edition, 2021, 60, 21502-21511.	13.8	45
25	Mesoporous Fe-doped MgO nanoparticles as a heterogeneous photo-Fenton-like catalyst for degradation of salicylic acid in wastewater. Journal of Environmental Chemical Engineering, 2021, 9, 105589.	6.7	22
26	New Mechanistic and Reaction Pathway Insights for Oxidative Coupling of Methane (OCM) over Supported Na 2 WO 4 /SiO 2 Catalysts. Angewandte Chemie, 2021, 133, 21672-21681.	2.0	3
27	Resolving the Types and Origin of Active Oxygen Species Present in Supported Mn-Na <sub>2</sub> WO <sub>4</sub> /SiO <sub>2</sub> Catalysts for Oxidative Coupling of Methane. ACS Catalysis, 2021, 11, 10288-10293.	11.2	29
28	Sulfur Tolerant Subnanometer Fe/Alumina Catalysts for Propane Dehydrogenation. ACS Applied Nano Materials, 2021, 4, 10055-10067.	5.0	13
29	The Often-Overlooked Power of Summary Statistics in Exploratory Data Analysis: Comparison of Pattern Recognition Entropy (PRE) to Other Summary Statistics and Introduction of Divided Spectrum-PRE (DS-PRE). Journal of Chemical Information and Modeling, 2021, 61, 4173-4189.	5.4	7
30	Atmospheric Pressure DBD Plasma Ammonia Synthesis and Separation Process Design and Environmental Impact Assessment. ACS Sustainable Chemistry and Engineering, 2021, 9, 13233-13244.	6.7	11
31	Systematic and collaborative approach to problem solving using X-ray photoelectron spectroscopy. Applied Surface Science Advances, 2021, 5, 100112.	6.8	451
32	Surface chemistry of hydroxyapatite for sustainable n-butanol production from bio-ethanol. Chem Catalysis, 2021, 1, 782-801.	6.1	9
33	Comprehensive process and environmental impact analysis of integrated DBD plasma steam methane reforming. Fuel, 2021, 304, 121328.	6.4	20
34	Towards a reliable assessment of charging effects during surface analysis: Accurate spectral shapes of ZrO2 and Pd/ZrO2 via X-ray Photoelectron Spectroscopy. Applied Surface Science, 2021, 566, 150728.	6.1	9
35	Destruction of emerging organophosphate contaminants in wastewater using the heterogeneous iron-based photo-Fenton-like process. Journal of Hazardous Materials Letters, 2021, 2, 100012.	3.6	11
36	Low concentrations of Cu <sup>2+</sup> in synthetic nutrient containing wastewater inhibit MgCO <sub>3</sub> -to-struvite transformation. Environmental Science: Water Research and Technology, 2021, 7, 521-534.	2.4	4

#	Article	IF	CITATIONS
37	Methane activation by ZSM-5-supported transition metal centers. Chemical Society Reviews, 2021, 50, 1251-1268.	38.1	77
38	First-principles-informed energy span and microkinetic analysis of ethanol catalytic conversion to 1,3-butadiene on MgO. Catalysis Science and Technology, 2021, 11, 6682-6694.	4.1	4
39	A combined computational and experimental study of methane activation during oxidative coupling of methane (OCM) by surface metal oxide catalysts. Chemical Science, 2021, 12, 14143-14158.	7.4	5
40	Atomically Dispersed Tin-Modified γ-alumina for Selective Propane Dehydrogenation under H <sub>2</sub> S Co-feed. ACS Catalysis, 2021, 11, 13472-13482.	11.2	8
41	Phosphate removal from simulated wastewater using industrial calcium-containing solid waste. Journal of Environmental Chemical Engineering, 2021, 9, 106575.	6.7	8
42	Transformation of Liquid Digestate from the Solid-Separated Biogas Digestion Reactor Effluent into a Solid NH <sub>4</sub> HCO <sub>3</sub> Fertilizer: Sustainable Process Engineering and Life Cycle Assessment. ACS Sustainable Chemistry and Engineering, 2021, 9, 580-588.	6.7	18
43	Solar Steam Generation Integration into the Ammonium Bicarbonate Recovery from Liquid Biomass Digestate: Process Modeling and Life Cycle Assessment. ACS Sustainable Chemistry and Engineering, 2021, 9, 15278-15286.	6.7	6
44	Curve fitting complex X-ray photoelectron spectra of graphite-supported copper nanoparticles using informed line shapes. Applied Surface Science, 2020, 505, 143841.	6.1	21
45	The quality and energy potential of introduced energy crops in northern part of temperate climate zone. Renewable Energy, 2020, 151, 887-895.	8.9	13
46	A review of phosphate adsorption on Mg-containing materials: kinetics, equilibrium, and mechanistic insights. Environmental Science: Water Research and Technology, 2020, 6, 3178-3194.	2.4	24
47	Transition metal-doped MgO nanoparticles for nutrient recycling: an alternate Mg source for struvite synthesis from wastewater. Environmental Science: Nano, 2020, 7, 3482-3496.	4.3	14
48	Granulated biofuel ash as a sustainable source of plant nutrients. Waste Management and Research, 2020, 39, 0734242X2094895.	3.9	11
49	Simultaneous Process Design of a Cooled Tubular Fischer–Tropsch Reactor. Energy Technology, 2020, 8, 2000683.	3.8	1
50	Superstructural diversity in salt-cocrystals: higher-order hydrogen-bonded assemblies formed using U-shaped dications and with assistance of Ï€ <sup>â~'</sup> –π stacking. Chemical Communications, 2020, 56, 6708-6710.	4.1	8
51	Relative Humidity Facilitated Urea Particle Reaction with Salicylic Acid: A Combined In Situ Spectroscopy and DFT Study. ACS Earth and Space Chemistry, 2020, 4, 1018-1028.	2.7	12
52	Existence and Properties of Isolated Catalytic Sites on the Surface of Î <sup>2</sup> -Cristobalite-Supported, Doped Tungsten Oxide Catalysts (WO <sub><i>x</i></sub> /Î <sup>2</sup> -SiO <sub>2</sub> ,) Tj ETQq0 0 0 rgBT /Overlock 10 Tf 50 Oxidative Coupling of Methane (OCM): A Combined Periodic DFT and Experimental Study. ACS Catalysis,	) 147 Td ( 11.2	Na-WO <sub> 33</sub>
53	2020, 10, 4580-4592. Deposition and properties of mixed molybdenum sulfide (MoS2) and copper sulfide (CuxS) films on glass surface using elemental sulfur as a precursor. Thin Solid Films, 2020, 709, 138209.	1.8	3
54	In situ monitoring of mechanochemical synthesis of calcium urea phosphate fertilizer cocrystal reveals highly effective water-based autocatalysis. Chemical Science, 2020, 11, 2350-2355.	7.4	40

#	Article	IF	CITATIONS
55	Anthracite coal-based activated carbon for elemental Hg adsorption in simulated flue gas: Preparation and evaluation. Fuel, 2020, 275, 117921.	6.4	32
56	Synthesis and molecular structure of model silica-supported tungsten oxide catalysts for oxidative coupling of methane (OCM). Catalysis Science and Technology, 2020, 10, 3334-3345.	4.1	35
57	Mechanochemically synthesized gypsum and gypsum drywall waste cocrystals with urea for enhanced environmental sustainability fertilizers. Journal of Environmental Chemical Engineering, 2020, 8, 103965.	6.7	13
58	Multifunctional Urea Cocrystal with Combined Ureolysis and Nitrification Inhibiting Capabilities for Enhanced Nitrogen Management. ACS Sustainable Chemistry and Engineering, 2019, 7, 13369-13378.	6.7	32
59	First-principles microkinetic study of methane and hydrogen sulfide catalytic conversion to methanethiol/dimethyl sulfide on Mo6S8 clusters: activity/selectivity of different promoters. Catalysis Science and Technology, 2019, 9, 4573-4580.	4.1	5
60	Methylated Poly(ethylene)imine Modified Capacitive Micromachined Ultrasonic Transducer for Measurements of CO2 and SO2 in Their Mixtures. Sensors, 2019, 19, 3236.	3.8	18
61	Inhibitor, Co-Catalyst, or Co-Reactant? Probing the Different Roles of H <sub>2</sub> S during CO <sub>2</sub> Hydrogenation on the MoS <sub>2</sub> Catalyst. ACS Catalysis, 2019, 9, 10044-10059.	11.2	24
62	Experimental Insights into the Genesis and Growth of Struvite Particles on Low-Solubility Dolomite Mineral Surfaces. Journal of Physical Chemistry C, 2019, 123, 25135-25145.	3.1	20
63	Oxidative Coupling of Methane (OCM) by SiO <sub>2</sub> -Supported Tungsten Oxide Catalysts Promoted with Mn and Na. ACS Catalysis, 2019, 9, 5912-5928.	11.2	136
64	CO <sub>2</sub> and SO <sub>2</sub> Interactions with Methylated Poly(ethylenimine)-Functionalized Capacitive Micromachined Ultrasonic Transducers (CMUTs): Gas Sensing and Degradation Mechanism. ACS Applied Electronic Materials, 2019, 1, 1150-1161.	4.3	14
65	Spatially Resolved Product Speciation during Struvite Synthesis from Magnesite (MgCO <sub>3</sub> ) Particles in Ammonium (NH <sub>4</sub> <sup>+</sup> ) and Phosphate (PO <sub>4</sub> <sup>3–</sup> ) Aqueous Solutions. Journal of Physical Chemistry C, 2019, 123, 8908-8922.	3.1	17
66	Mechanochemical Synthesis of Ca- and Mg-Double Salt Crystalline Materials Using Insoluble Alkaline Earth Metal Bearing Minerals. ACS Sustainable Chemistry and Engineering, 2019, 7, 6802-6812.	6.7	13
67	The shape-dependent surface oxidation of 2D ultrathin Mo2C crystals. Nanoscale Advances, 2019, 1, 4692-4696.	4.6	7
68	Novel Dual-Action Plant Fertilizer and Urease Inhibitor: UreaÂ-Catechol Cocrystal. Characterization and Environmental Reactivity. ACS Sustainable Chemistry and Engineering, 2019, 7, 2852-2859.	6.7	42
69	Transient Struvite Formation during Stoichiometric (1:1) NH <sub>4</sub> <sup>+</sup> and PO <sub>4</sub> <sup>3–</sup> Adsorption/Reaction on Magnesium Oxide (MgO) Particles. ACS Sustainable Chemistry and Engineering, 2019, 7, 1545-1556.	6.7	30
70	Critical review on the active site structure of sulfated zirconia catalysts and prospects in fuel production. Applied Catalysis A: General, 2019, 572, 210-225.	4.3	69
71	<i>Operando</i> Structure Determination of Cu and Zn on Supported MgO/SiO <sub>2</sub> Catalysts during Ethanol Conversion to 1,3-Butadiene. ACS Catalysis, 2019, 9, 269-285.	11.2	38
72	Reactive Mechanosynthesis of Urea Ionic Cocrystal Fertilizer Materials from Abundant Low Solubility Magnesium- and Calcium-Containing Minerals. ACS Sustainable Chemistry and Engineering, 2018, 6, 4680-4687.	6.7	28

#	Article	IF	CITATIONS
73	Electrooxidation of Glycerol on Gold in Acidic Medium: A Combined Experimental and DFT Study. Journal of Physical Chemistry C, 2018, 122, 10489-10494.	3.1	32
74	Design of a separation section in an ethanol-to-butanol process. Biomass and Bioenergy, 2018, 109, 231-238.	5.7	23
75	Molecular structure and sour gas surface chemistry of supported K2O/WO3/Al2O3 catalysts. Applied Catalysis B: Environmental, 2018, 232, 146-154.	20.2	19
76	Structure and Vibrational Properties of Potassium-Promoted Tungsten Oxide Catalyst Monomeric Sites Supported on Alumina (K2O/WO3/Al2O3) Characterized Using Periodic Density Functional Theory. Journal of Physical Chemistry C, 2018, 122, 24190-24201.	3.1	11
77	Carnallite-Derived Solid Waste as Potassium (K) and Magnesium (Mg) Source in Granulated Compound NPK Fertilizers. ACS Sustainable Chemistry and Engineering, 2018, 6, 9427-9433.	6.7	12
78	In Situ Spectroscopic Insights on the Molecular Structure of the MgO/SiO <sub>2</sub> Catalytic Active Sites during Ethanol Conversion to 1,3-Butadiene. Journal of Physical Chemistry C, 2018, 122, 20894-20906.	3.1	30
79	Smart urea ionic co-crystals with enhanced urease inhibition activity for improved nitrogen cycle management. Chemical Communications, 2018, 54, 7637-7640.	4.1	41
80	Spectroscopic and Microscopic Identification of the Reaction Products and Intermediates during the Struvite (MgNH <sub>4</sub> PO <sub>4</sub> ·6H <sub>2</sub> O) Formation from Magnesium Oxide (MgO) and Magnesium Carbonate (MgCO <sub>3</sub> ) Microparticles. ACS Sustainable Chemistry and Engineering, 2017, 5, 1567-1577.	6.7	44
81	Minireview: direct catalytic conversion of sour natural gas (CH <sub>4</sub> + H <sub>2</sub> S +) Tj ETQq1 1 2017, 7, 2919-2929.	0.784314 4.1	rgBT /Overloc 34
82	Design and control of a cryogenic multi-stage compression refrigeration process. Chemical Engineering Research and Design, 2017, 121, 360-367.	5.6	27
83	Adjustable N:P <sub>2</sub> O <sub>5</sub> Ratio Urea Phosphate Fertilizers for Sustainable Phosphorus and Nitrogen Use: Liquid Phase Equilibria via Solubility Measurements and Raman Spectroscopy. ACS Sustainable Chemistry and Engineering, 2017, 5, 1747-1754.	6.7	11
84	Catalytic conversion of ethanol to 1,3-butadiene on MgO: A comprehensive mechanism elucidation using DFT calculations. Journal of Catalysis, 2017, 346, 78-91.	6.2	70
85	Surface chemistry of MgO/SiO <sub>2</sub> catalyst during the ethanol catalytic conversion to 1,3-butadiene: in-situ DRIFTS and DFT study. Catalysis Science and Technology, 2017, 7, 4648-4668.	4.1	58
86	Mechanosynthesis of Magnesium and Calcium Salt–Urea Ionic Cocrystal Fertilizer Materials for Improved Nitrogen Management. ACS Sustainable Chemistry and Engineering, 2017, 5, 8546-8550.	6.7	55
87	CH4 and H2S reforming to CH3SH and H2 catalyzed by metal-promoted Mo6S8 clusters: a first-principles micro-kinetic study. Catalysis Science and Technology, 2017, 7, 3546-3554.	4.1	10
88	Sustainable Ammonia Production. ACS Sustainable Chemistry and Engineering, 2017, 5, 9527-9527.	6.7	74
89	Efficiency Evaluation of Dairy Wastewater Derived Zinc Micronutrient Containing Sustainable Fertilizers. ACS Sustainable Chemistry and Engineering, 2017, 5, 6692-6699.	6.7	9
90	Chemical and structural changes in polyamide based organic–inorganic hybrid materials upon incorporation of SeS2O62â~' precursor. Applied Surface Science, 2017, 392, 634-641.	6.1	10

#	Article	IF	CITATIONS
91	Bactericidal effect of graphene oxide/Cu/Ag nanoderivatives against Escherichia coli , Pseudomonas aeruginosa , Klebsiella pneumoniae , Staphylococcus aureus and Methicillin-resistant Staphylococcus aureus. International Journal of Pharmaceutics, 2016, 511, 90-97.	5.2	42
92	Chemical routes to hydrocarbons from pyrolysis of lignocellulose using Cs promoted amorphous silica alumina catalyst. Catalysis Today, 2016, 269, 156-165.	4.4	26
93	From Insoluble Minerals to Liquid Fertilizers: Magnesite as a Source of Magnesium (Mg) Nutrient. ACS Sustainable Chemistry and Engineering, 2016, 4, 5404-5408.	6.7	9
94	Surface chemistry of carbon dioxide revisited. Surface Science Reports, 2016, 71, 595-671.	7.2	132
95	Molecular and Morphological Structure of Poultry Manure Derived Organo-Mineral Fertilizers (OMFs). ACS Sustainable Chemistry and Engineering, 2016, 4, 4788-4796.	6.7	11
96	Hematite decorated multi-walled carbon nanotubes (α-Fe2O3/MWCNTs) as sorbents for Cu(ii) and Cr(vi): comparison of hybrid sorbent performance to its nanomaterial building blocks. RSC Advances, 2016, 6, 99997-100007.	3.6	21
97	Greenhouse Gas Molecule CO <sub>2</sub> Detection Using a Capacitive Micromachined Ultrasound Transducer. Analytical Chemistry, 2016, 88, 6662-6665.	6.5	21
98	Efficient photocatalytic hydrogen evolution system by assembling earth abundant NixOy nanoclusters in cubic MCM-48 mesoporous materials. RSC Advances, 2016, 6, 59169-59180.	3.6	8
99	CH 4 conversion to value added products: Potential, limitations and extensions of a single step heterogeneous catalysis. Applied Catalysis B: Environmental, 2016, 198, 525-547.	20.2	185
100	Characterization of urea derived polymeric carbon nitride and resultant thermally vacuum deposited amorphous thin films: Structural, chemical and photophysical properties. Carbon, 2016, 107, 415-425.	10.3	22
101	Comparative life cycle assessment of plasma-based and traditional exhaust gas treatment technologies. Journal of Cleaner Production, 2016, 112, 1804-1812.	9.3	47
102	Engineered Pelletized Organo-Mineral Fertilizers (OMF) from Poultry Manure, Diammonium Phosphate and Potassium Chloride. ACS Sustainable Chemistry and Engineering, 2016, 4, 2279-2285.	6.7	30
103	Dairy Wastewater for Production of Chelated Biodegradable Zn Micronutrient Fertilizers. ACS Sustainable Chemistry and Engineering, 2016, 4, 1722-1727.	6.7	12
104	Solar hydrogen generation over CdS incorporated in Ti-MCM-48 mesoporous materials under visible light illumination. International Journal of Hydrogen Energy, 2016, 41, 4106-4119.	7.1	19
105	Reversible Photohydration of Trenbolone Acetate Metabolites: Mechanistic Understanding of Product-to-Parent Reversion through Complementary Experimental and Theoretical Approaches. Environmental Science & Technology, 2016, 50, 6753-6761.	10.0	14
106	Catalytic methyl mercaptan coupling to ethylene in chabazite: DFT study of the first C C bond formation. Applied Catalysis B: Environmental, 2016, 187, 195-203.	20.2	13
107	Geometry and Electronic Properties of Glycerol Adsorbed on Bare and Transition-Metal Surface-Alloyed Au(111): A Density Functional Theory Study. Journal of Physical Chemistry C, 2016, 120, 1749-1757.	3.1	18
108	Urea–Ammonium Nitrate Aqueous Solutions Containing Cu Micronutrient Obtained from Cable Manufacturing Solid Waste. ACS Sustainable Chemistry and Engineering, 2015, 3, 1544-1550.	6.7	8

Jonas Baltrusaitis

#	Article	IF	CITATIONS
109	Structural, chemical and optical properties of the polyethylene–copper sulfide composite thin films synthesized using polythionic acid as sulfur source. Applied Surface Science, 2015, 347, 520-527.	6.1	6
110	Modification of polyamide-CdS-CdSe composite material films with Ag using a cation–cation exchange reaction. Applied Surface Science, 2015, 351, 203-208.	6.1	4
111	Cycloexpansamines A and B: spiroindolinone alkaloids from a marine isolate of Penicillium sp. (SF-5292). Journal of Antibiotics, 2015, 68, 715-718.	2.0	18
112	CMUT for high sensitivity greenhouse gas sensing. , 2015, , .		5
113	Combination of Argentophilic and Perfluorophenyl-Perfluorophenyl Interactions Supports a Head-to-Head [2 + 2] Photodimerization in the Solid State. Crystal Growth and Design, 2015, 15, 538-541.	3.0	48
114	Structure, morphology and electrochemical properties of zinc–cobalt oxide films on AISI 304 type steel. Journal of Applied Electrochemistry, 2015, 45, 405-417.	2.9	10
115	Solar simulated hydrogen evolution using cobalt oxide nanoclusters deposited on titanium dioxide mesoporous materials prepared by evaporation induced self-assembly process. International Journal of Hydrogen Energy, 2015, 40, 10795-10806.	7.1	9
116	Phase Composition of Aqueous Urea–Ammonium Nitrate (UAN)–Zinc Nitrate Solutions for Sustainable Reuse of Zinc Containing Industrial Pigment Waste. ACS Sustainable Chemistry and Engineering, 2015, 3, 950-958.	6.7	13
117	Electro-oxidation of water on hematite: Effects of surface termination and oxygen vacancies investigated by first-principles. Surface Science, 2015, 640, 45-49.	1.9	43
118	Characterization of linear alkyl phosphonate self-assembled on perovskite substrate. Applied Surface Science, 2015, 344, 159-162.	6.1	4
119	Electrochemically Deposited Sb and In Doped Tin Sulfide (SnS) Photoelectrodes. Journal of Physical Chemistry C, 2015, 119, 6471-6480.	3.1	27
120	Methane Conversion to Syngas for Gas-to-Liquids (GTL): Is Sustainable CO <sub>2</sub> Reuse via Dry Methane Reforming (DMR) Cost Competitive with SMR and ATR Processes?. ACS Sustainable Chemistry and Engineering, 2015, 3, 2100-2111.	6.7	80
121	Pd–Ti-MCM-48 cubic mesoporous materials for solar simulated hydrogen evolution. International Journal of Hydrogen Energy, 2015, 40, 905-918.	7.1	21
122	Generalized molybdenum oxide surface chemical state XPS determination via informed amorphous sample model. Applied Surface Science, 2015, 326, 151-161.	6.1	375
123	Deposition, structure and properties of polyamide–CdSe–CdS composite material using sorption–diffusion method. Applied Surface Science, 2015, 325, 175-184.	6.1	4
124	Photocatalytic decomposition of cortisone acetate in aqueous solution. Journal of Hazardous Materials, 2015, 282, 208-215.	12.4	29
125	Decomposition of 2-naphthol in water using a non-thermal plasma reactor. Chemical Engineering Journal, 2015, 260, 188-198.	12.7	42
126	Design and Characterization of Electrospun Polyamide Nanofiber Media for Air Filtration Applications. Journal of Nanomaterials, 2014, 2014, 1-13.	2.7	101

#	Article	IF	CITATIONS
127	Characterization of Plasma Polymerized Hexamethyldisiloxane Films Prepared by Arc Discharge. Plasma Chemistry and Plasma Processing, 2014, 34, 271-285.	2.4	14
128	Photocatalytic degradation of dye by Ag/ZnO prepared by reduction of Tollen's reagent and the ecotoxicity of degraded products. Korean Journal of Chemical Engineering, 2014, 31, 587-592.	2.7	28
129	Iron oxide nanoparticles induce Pseudomonas aeruginosa growth, induce biofilm formation, and inhibit antimicrobial peptide function. Environmental Science: Nano, 2014, 1, 123.	4.3	96
130	Nanocrystals of a Metal–Organic Complex Exhibit Remarkably High Conductivity that Increases in a Single-Crystal-to-Single-Crystal Transformation. Journal of the American Chemical Society, 2014, 136, 6778-6781.	13.7	92
131	Ag2S deposited on oxidized polypropylene as composite material for solar light absorption. Applied Surface Science, 2014, 301, 134-141.	6.1	27
132	Absolute Organic Crystal Thermodynamics: Growth of the Asymmetric Unit into a Crystal via Alchemy. Journal of Chemical Theory and Computation, 2014, 10, 2781-2791.	5.3	24
133	Competitive role of structural properties of titania–silica mixed oxides and a mechanistic study of the photocatalytic degradation of phenol. Applied Catalysis B: Environmental, 2014, 148-149, 394-405.	20.2	41
134	Photoelectrochemical Hydrogen Production on αâ€Fe <sub>2</sub> O <sub>3</sub> (0001): Insights from Theory and Experiments. ChemSusChem, 2014, 7, 162-171.	6.8	27
135	Insight into band positions and inter-particle electron transfer dynamics between CdS nanoclusters and spatially isolated TiO <sub>2</sub> dispersed in cubic MCM-48 mesoporous materials: a highly efficient system for photocatalytic hydrogen evolution under visible light illumination. Physical Chemistry Chemical Physics. 2014. 16. 2048-2061.	2.8	17
136	Heterogeneous Reactivity of Nitric Acid with Nascent Sea Spray Aerosol: Large Differences Observed between and within Individual Particles. Journal of Physical Chemistry Letters, 2014, 5, 2493-2500.	4.6	66
137	Thermally-driven structural changes of graphene oxide multilayer films deposited on glass substrate. Superlattices and Microstructures, 2014, 75, 461-467.	3.1	13
138	Renewable energy based catalytic CH4 conversion to fuels. Catalysis Science and Technology, 2014, 4, 2397.	4.1	66
139	Liquid and Solid Compound Granulated Diurea Sulfate-Based Fertilizers for Sustainable Sulfur Source. ACS Sustainable Chemistry and Engineering, 2014, 2, 2477-2487.	6.7	17
140	N-Functionalized Carbon Nanotubes As a Source and Precursor of <i>N</i> -Nitrosodimethylamine: Implications for Environmental Fate, Transport, and Toxicity. Environmental Science & Technology, 2014, 48, 9279-9287.	10.0	23
141	High Throughput Analysis of Photocatalytic Water Purification. Analytical Chemistry, 2014, 86, 7612-7617.	6.5	10
142	Polyamide–thallium selenide composite materials via temperature and pH controlled adsorption–diffusion method. Applied Surface Science, 2014, 317, 818-827.	6.1	8
143	Surface Photochemistry of Adsorbed Nitrate: The Role of Adsorbed Water in the Formation of Reduced Nitrogen Species on α-Fe <sub>2</sub> O <sub>3</sub> Particle Surfaces. Journal of Physical Chemistry A, 2014, 118, 158-166.	2.5	75
144	Electrochemical CO <sub>2</sub> reduction on Cu <sub>2</sub> O-derived copper nanoparticles: controlling the catalytic selectivity of hydrocarbons. Physical Chemistry Chemical Physics, 2014, 16, 12194-12201.	2.8	458

#	Article	IF	CITATIONS
145	Effects of bismuth addition and photo-deposition of platinum on (surface) composition, morphology and visible light photocatalytic activity of sol–gel derived TiO2. Applied Catalysis B: Environmental, 2014, 154-155, 153-160.	20.2	18
146	Noncentrosymmetric Packings Influenced by Electronic Properties of Products of Click Reactions. Crystal Growth and Design, 2014, 14, 893-896.	3.0	3
147	Water adsorption constrained Frenkel–Halsey–Hill adsorption activation theory: Montmorillonite and illite. Atmospheric Environment, 2014, 87, 26-33.	4.1	31
148	Water droplet behavior on superhydrophobic SiO2 nanocomposite films during icing/deicing cycles. Materials Characterization, 2013, 82, 9-16.	4.4	65
149	Synthesis-Dependent Oxidation State of Platinum on TiO <sub>2</sub> and Their Influences on the Solar Simulated Photocatalytic Hydrogen Production from Water. Journal of Physical Chemistry C, 2013, 117, 16850-16862.	3.1	40
150	Status and perspectives of CO2 conversion into fuels and chemicals by catalytic, photocatalytic and electrocatalytic processes. Energy and Environmental Science, 2013, 6, 3112.	30.8	1,475
151	Heterogeneous Uptake and Adsorption of Gas-Phase Formic Acid on Oxide and Clay Particle Surfaces: The Roles of Surface Hydroxyl Groups and Adsorbed Water in Formic Acid Adsorption and the Impact of Formic Acid Adsorption on Water Uptake. Journal of Physical Chemistry A, 2013, 117, 11316-11327.	2.5	43
152	Selective Hydrothermal Method To Create Patterned and Photoelectrochemically Effective Pt/WO <sub>3</sub> Interfaces. ACS Applied Materials & Interfaces, 2013, 5, 13050-13054.	8.0	9
153	Synthesis and characterization of ligand stabilized CdS-Trititanate composite materials for visible light-induced photocatalytic water splitting. International Journal of Hydrogen Energy, 2013, 38, 2656-2669.	7.1	23
154	Influence of Ti–O–Si hetero-linkages in the photocatalytic degradation of Rhodamine B. Catalysis Communications, 2013, 31, 66-70.	3.3	54
155	Synthesis and surface properties of polyamide-CuxSe composite thin films. Applied Surface Science, 2013, 283, 360-366.	6.1	24
156	Effect of Phosphate Salts (Na <sub>3</sub> PO <sub>4</sub> , Na <sub>2</sub> HPO <sub>4</sub> , and) Tj ETQq Photocatalytic Dye Degradation under Visible Light and Toxicity of the Degraded Dye Products. Industrial & amp; Engineering Chemistry Research, 2013, 52, 17369-17375.	0 0 0 rgBT 3.7	/Overlock 1 71
157	Tribological properties of the two-step thermally deposited chromium films. Applied Surface Science, 2013, 283, 1089-1095.	6.1	2
158	Polyvinylpyrrolidone surface modification with SiOx containing amorphous hydrogenated carbon (a-C:H/SiOx) and nitrogen-doped a-C:H/SiOx films using Hall-type closed drift ion beam source. Thin Solid Films, 2013, 538, 25-31.	1.8	8
159	Exploration of the role of anions in the synthesis of Cr containing mesoporous materials at room temperature. Microporous and Mesoporous Materials, 2013, 170, 211-225.	4.4	6
160	Investigation of the role of platinum oxide for the degradation of phenol under simulated solar irradiation. Applied Catalysis B: Environmental, 2013, 136-137, 248-259.	20.2	19
161	Ultra-stable CdS incorporated Ti-MCM-48 mesoporous materials for efficient photocatalytic decomposition of water under visible light illumination. Chemical Communications, 2013, 49, 3221.	4.1	64
162	Horizontal Attenuated Total Reflectance Fourier Transform Infrared and X-ray Photoelectron Spectroscopy Measurements of Water Adsorption on Oxidized Tin(II) Sulfide (SnS) Surfaces. Journal of Physical Chemistry C, 2013, 117, 472-482.	3.1	6

#	Article	IF	CITATIONS
163	Surface morphology, cohesive and adhesive properties of amorphous hydrogenated carbon nanocomposite films. Applied Surface Science, 2013, 276, 543-549.	6.1	10
164	Transition Metal Sulfide Hydrogen Evolution Catalysts for Hydrobromic Acid Electrolysis. Langmuir, 2013, 29, 480-492.	3.5	81
165	Synthesis and properties of polyamide–Ag2S composite based solar energy absorber surfaces. Applied Surface Science, 2013, 282, 552-560.	6.1	14
166	Size-Dependent Changes in Sea Spray Aerosol Composition and Properties with Different Seawater Conditions. Environmental Science & amp; Technology, 2013, 47, 5603-5612.	10.0	175
167	Phenomenon of Quantum Entanglement in a System Composed of Two Minimal Protocells. Origins of Life and Evolution of Biospheres, 2013, 43, 49-66.	1.9	4
168	Identification and Environmental Implications of Photo-Transformation Products of Trenbolone Acetate Metabolites. Environmental Science & Technology, 2013, 47, 5031-5041.	10.0	47
169	Inside versus Outside: Ion Redistribution in Nitric Acid Reacted Sea Spray Aerosol Particles as Determined by Single Particle Analysis. Journal of the American Chemical Society, 2013, 135, 14528-14531.	13.7	89
170	Effects of Eyjafjallajökull Volcanic Ash on Innate Immune System Responses and Bacterial Growth <i>in Vitro</i> . Environmental Health Perspectives, 2013, 121, 691-698.	6.0	29
171	Bringing the ocean into the laboratory to probe the chemical complexity of sea spray aerosol. Proceedings of the National Academy of Sciences of the United States of America, 2013, 110, 7550-7555.	7.1	439
172	Product-to-Parent Reversion of Trenbolone: Unrecognized Risks for Endocrine Disruption. Science, 2013, 342, 347-351.	12.6	73
173	H <sub>2</sub> Sâ€Mediated Thermal and Photochemical Methane Activation. ChemPhysChem, 2013, 14, 3960-3970.	2.1	9
174	Coal Fly Ash Impairs Airway Antimicrobial Peptides and Increases Bacterial Growth. PLoS ONE, 2013, 8, e57673.	2.5	27
175	Influenza A Viral Replication Is Blocked by Inhibition of the Inositol-requiring Enzyme 1 (IRE1) Stress Pathway. Journal of Biological Chemistry, 2012, 287, 4679-4689.	3.4	122
176	Endoplasmic Reticulum Stress, A Potential Therapeutic Target For Influenza A Viral Infection. , 2012, , .		0
177	Preservation of York Minster historic limestone by hydrophobic surface coatings. Scientific Reports, 2012, 2, 880.	3.3	23
178	Visible light driven photocatalytic evolution of hydrogen from water over CdS encapsulated MCM-48 materials. RSC Advances, 2012, 2, 5754.	3.6	53
179	Scope of Stereoselective Mn-Mediated Radical Addition to Chiral Hydrazones and Application in a Formal Synthesis of Quinine. Journal of Organic Chemistry, 2012, 77, 3159-3180.	3.2	35
180	Formation of Iron(III) (Hydr)oxides on Polyaspartate- and Alginate-Coated Substrates: Effects of Coating Hydrophilicity and Functional Group. Environmental Science & Technology, 2012, 46, 13167-13175.	10.0	31

Jonas Baltrusaitis

#	Article	IF	CITATIONS
181	Computational Studies of CO <sub>2</sub> Activation via Photochemical Reactions with Reduced Sulfur Compounds. Journal of Physical Chemistry A, 2012, 116, 9331-9339.	2.5	25
182	Coal Fly Ash as a Source of Iron in Atmospheric Dust. Environmental Science & Technology, 2012, 46, 2112-2120.	10.0	129
183	Organic Nanocrystals of the Resorcinarene Hexamer via Sonochemistry: Evidence of Reversed Crystal Growth Involving Hollow Morphologies. Journal of the American Chemical Society, 2012, 134, 6900-6903.	13.7	36
184	Electronic Properties and Reactivity of Simulated Fe <sup>3+</sup> and Cr <sup>3+</sup> Substituted α-Al <sub>2</sub> O <sub>3</sub> (0001) Surface. Journal of Physical Chemistry C, 2012, 116, 18847-18856.	3.1	23
185	Periodic DFT Study of Acidic Trace Atmospheric Gas Molecule Adsorption on Ca- and Fe-Doped MgO(001) Surface Basic Sites. Journal of Physical Chemistry A, 2012, 116, 7950-7958.	2.5	17
186	Aflaquinolones A–G: Secondary Metabolites from Marine and Fungicolous Isolates of <i>Aspergillus</i> spp Journal of Natural Products, 2012, 75, 464-472.	3.0	54
187	Water Adsorption on Clay Minerals As a Function of Relative Humidity: Application of BET and Freundlich Adsorption Models. Langmuir, 2012, 28, 1790-1803.	3.5	202
188	Heterogeneous Atmospheric Chemistry of Lead Oxide Particles with Nitrogen Dioxide Increases Lead Solubility: Environmental and Health Implications. Environmental Science & Technology, 2012, 46, 12806-12813.	10.0	50
189	Optimal experimental conditions for hydrogen production using low voltage electrooxidation of organic wastewater feedstock. International Journal of Hydrogen Energy, 2012, 37, 13304-13313.	7.1	14
190	Pharmaceutical Applications of the Polarizable Amoeba Potential, Including Protein-Ligand Binding Affinity and Drug Solubility, using the Force Field X Software. Biophysical Journal, 2012, 102, 409a-410a.	0.5	0
191	Organic nanocrystals of [2.2]paracyclophanes achieved via sonochemistry: enhanced and red-shifted emission involving edge-to-face chromophores. CrystEngComm, 2012, 14, 7567.	2.6	8
192	Atomic Force Microscopy and X-ray Photoelectron Spectroscopy Study of NO <sub>2</sub> Reactions on CaCO <sub>3</sub> (10114) Surfaces in Humid Environments. Journal of Physical Chemistry A, 2012, 116, 9001-9009.	2.5	24
193	Dissolution of Hematite Nanoparticle Aggregates: Influence of Primary Particle Size, Dissolution Mechanism, and Solution pH. Langmuir, 2012, 28, 15797-15808.	3.5	83
194	The Structure, Thermodynamics, and Solubility of Organic Crystals from Simulation with a Polarizable Force Field. Journal of Chemical Theory and Computation, 2012, 8, 1721-1736.	5.3	77
195	Surface Chemistry of α-FeOOH Nanorods and Microrods with Gas-Phase Nitric Acid and Water Vapor: Insights into the Role of Particle Size, Surface Structure, and Surface Hydroxyl Groups in the Adsorption and Reactivity of α-FeOOH with Atmospheric Gases. Journal of Physical Chemistry C, 2012, 116. 12566-12577.	3.1	43
196	Enhanced photocatalytic water splitting activity of carbon-modified TiO2 composite materials synthesized by a green synthetic approach. International Journal of Hydrogen Energy, 2012, 37, 8257-8267.	7.1	101
197	Scaling down lateral dimensions of silicon nanopillars fabricated by reactive ion etching with Au/Cr self-assembled clusters as an etch mask. Thin Solid Films, 2012, 520, 2041-2045.	1.8	2
198	Atomic force microscopy and X-ray photoelectron spectroscopy evaluation of adhesion and nanostructure of thin Cr films. Thin Solid Films, 2012, 520, 6328-6333.	1.8	22

#	Article	IF	CITATIONS
199	Synthesis, characterization, photocatalytic and antibacterial activities of Ag-doped ZnO powders modified with a diblock copolymer. Powder Technology, 2012, 219, 158-164.	4.2	110
200	New phomactin analogues from an unidentified fungicolous fungal isolate obtained from the surface of a polypore. Planta Medica, 2012, 78, .	1.3	0
201	Sulfur Dioxide Adsorption on TiO <sub>2</sub> Nanoparticles: Influence of Particle Size, Coadsorbates, Sample Pretreatment, and Light on Surface Speciation and Surface Coverage. Journal of Physical Chemistry C, 2011, 115, 492-500.	3.1	91
202	Induction of Inflammasome-dependent Pyroptosis by Carbon Black Nanoparticles. Journal of Biological Chemistry, 2011, 286, 21844-21852.	3.4	162
203	Sulfur Dioxide Adsorption on ZnO Nanoparticles and Nanorods. Journal of Physical Chemistry C, 2011, 115, 10164-10172.	3.1	68
204	Thixotropic Hydrogel Derived from a Product of an Organic Solid-State Synthesis: Properties and Densities of Metalâ^'Organic Nanoparticles. Journal of the American Chemical Society, 2011, 133, 3365-3371.	13.7	91
205	Phomalevones Aâ^'C: Dimeric and Pseudodimeric Polyketides from a Fungicolous Hawaiian Isolate of <i>Phoma</i> sp. (Cucurbitariaceae). Journal of Natural Products, 2011, 74, 395-401.	3.0	42
206	Formation of paratacamite nanomaterials via the conversion of aged and oxidized copper nanoparticles in hydrochloric acidic media. Journal of Materials Chemistry, 2011, 21, 3162.	6.7	42
207	Ash From The Icelandic Eyjafjallajokull Volcano Inhibits Autophagy And Increases Stress Responses In Alveolar Macrophages. , 2011, , .		0
208	Electrochemical Deposition of Porous Cobalt Oxide Films on AISI 304 Type Steel. Medziagotyra, 2011, 17,	0.2	7
209	Synthesis and Characterization of Chlorine and Bromine Doped TiO <sub>2</sub> Nanoparticles for Photocatalytic Methanol Production. Microscopy and Microanalysis, 2011, 17, 1704-1705.	0.4	2
210	Semiconducting Organic Assemblies Prepared from Tetraphenylethylene Tetracarboxylic Acid and Bis(pyridine)s via Charge-Assisted Hydrogen Bonding. Journal of the American Chemical Society, 2011, 133, 8490-8493.	13.7	76
211	Layered molybdenum oxide thin films electrodeposited from sodium citrate electrolyte solution. Journal of Solid State Electrochemistry, 2011, 15, 711-723.	2.5	26
212	Radio frequency glow dischargeâ€induced acidification of fluoropolymers. Journal of Biomedical Materials Research - Part A, 2011, 99A, 418-425.	4.0	0
213	Carbon dioxide adsorption on oxide nanoparticle surfaces. Chemical Engineering Journal, 2011, 170, 471-481.	12.7	247
214	Crystal engineering rescues a solution organic synthesis in a cocrystallization that confirms the configuration of a molecular ladder. Proceedings of the National Academy of Sciences of the United States of America, 2011, 108, 10974-10979.	7.1	29
215	Electrically conductive surface modifications of three-dimensional polypropylene fumarate scaffolds. Journal of Biological Regulators and Homeostatic Agents, 2011, 25, S15-23.	0.7	4
216	Photoactive WO3 and Se-WO3 thin films for photoelectrochemical oxidation of organic compounds. Journal of Applied Electrochemistry, 2010, 40, 1337-1347.	2.9	6

#	Article	IF	CITATIONS
217	Low-Cost ZnO-Based Ultraviolet–Infrared Dual-Band Detector Sensitized With PbS Quantum Dots. IEEE Transactions on Electron Devices, 2010, 57, 2756-2760.	3.0	5
218	Supramolecular Catalysis in the Organic Solid State through Dry Grinding. Angewandte Chemie - International Edition, 2010, 49, 4273-4277.	13.8	115
219	A Red Zwitterionic Co-Crystal of Acetaminophen and 2,4-Pyridinedicarboxylic Acid. Journal of Pharmaceutical Sciences, 2010, 99, 3676-3683.	3.3	29
220	E-beam lithography of computer generated holograms using a fully vectorial 3D beam propagation method. Microelectronic Engineering, 2010, 87, 2332-2337.	2.4	7
221	The development of electrically conductive polycaprolactone fumarate–polypyrrole composite materials for nerve regeneration. Biomaterials, 2010, 31, 5916-5926.	11.4	132
222	Development of Electrically Conductive Oligo(polyethylene glycol) Fumarate-Polypyrrole Hydrogels for Nerve Regeneration. Biomacromolecules, 2010, 11, 2845-2853.	5.4	108
223	A template-free, thermal decomposition method to synthesize mesoporous MgO with a nanocrystalline framework and its application in carbon dioxide adsorption. Journal of Materials Chemistry, 2010, 20, 8705.	6.7	142
224	Reactions on Atmospheric Dust Particles: Surface Photochemistry and Size-Dependent Nanoscale Redox Chemistry. Journal of Physical Chemistry Letters, 2010, 1, 1729-1737.	4.6	74
225	Hymenopsins A and B and a Macrophorin Analogue from a Fungicolous <i>Hymenopsis</i> sp Journal of Natural Products, 2010, 73, 404-408.	3.0	19
226	Carbonic Acid Formation from Reaction of Carbon Dioxide and Water Coordinated to Al(OH) <sub>3</sub> : A Quantum Chemical Study. Journal of Physical Chemistry A, 2010, 114, 2350-2356.	2.5	37
227	Plasma etching of virtually stress-free stacked silicon nitride films. Thin Solid Films, 2009, 517, 5769-5772.	1.8	5
228	Calcite surface in humid environments. Surface Science, 2009, 603, L99-L104.	1.9	37
229	Dramatic Red-Shifted Fluorescence of [2.2]Paracyclophanes with Peripheral Substituents Attached to the Saturated Bridges. Organic Letters, 2009, 11, 5106-5109.	4.6	21
230	Synthesis of sub-wavelength diffractive optical elements by 3D full-vectorial beam propagation method. , 2009, , .		0
231	XPS study of nitrogen dioxide adsorption on metal oxide particle surfaces under different environmental conditions. Physical Chemistry Chemical Physics, 2009, 11, 8295.	2.8	241
232	1,4-Bis(phosphine)-2,5-difluoro-3,6-dihydroxybenzenes and their P-oxides: Syntheses, structures, ligating and electronic properties. Journal of Organometallic Chemistry, 2008, 693, 3263-3272.	1.8	16
233	A thin chromium film formation monitoring method: Monitoring of the early stages. Thin Solid Films, 2008, 516, 2943-2947.	1.8	7
234	A study of stacked PECVD silicon nitride films used for surface micromachined membranes. Thin Solid Films, 2008, 516, 8788-8792.	1.8	13

#	Article	IF	CITATIONS
235	Characterization and acidâ€mobilization study of ironâ€containing mineral dust source materials. Journal of Geophysical Research, 2008, 113, .	3.3	139
236	FTIR spectroscopy combined with quantum chemical calculations to investigate adsorbed nitrate on aluminium oxide surfaces in the presence and absence of co-adsorbed water. Physical Chemistry Chemical Physics, 2007, 9, 4970.	2.8	119
237	Reactions of sulfur dioxide on calcium carbonate single crystal and particle surfaces at the adsorbed water carbonate interface. Physical Chemistry Chemical Physics, 2007, 9, 3011.	2.8	156
238	Adsorption of sulfur dioxide on hematite and goethite particle surfaces. Physical Chemistry Chemical Physics, 2007, 9, 5542.	2.8	303
239	Surface Reactions of Carbon Dioxide at the Adsorbed Waterâ^'Oxide Interface. Journal of Physical Chemistry C, 2007, 111, 14870-14880.	3.1	69
240	Spatially Resolved Product Formation in the Reaction of Formic Acid with Calcium Carbonate (101Ì,,4):Â The Role of Step Density and Adsorbed Water-Assisted Ion Mobility. Langmuir, 2007, 23, 7039-7045.	3.5	23
241	A Spectroscopic Study of Atmospherically Relevant Concentrated Aqueous Nitrate Solutions. Journal of Physical Chemistry A, 2007, 111, 544-548.	2.5	59
242	Sialolith Characterization by Scanning Electron Microscopy and X-ray Photoelectron Spectroscopy. Scanning, 2007, 29, 206-210.	1.5	12
243	FTIR Spectroscopy Combined with Isotope Labeling and Quantum Chemical Calculations to Investigate Adsorbed Bicarbonate Formation Following Reaction of Carbon Dioxide with Surface Hydroxyl Groups on Fe2O3and Al2O3. Journal of Physical Chemistry B, 2006, 110, 12005-12016.	2.6	170
244	Chemical Properties of Oxide Nanoparticles: Surface Adsorption Studies from Gas- and Liquid-Phase Environments. , 2006, , 335-351.		2
245	Reactivity of Formic Acid on Calcium Carbonate Single Particle and Single Crystal Surfaces: Effect of Adsorbed Water. Microscopy and Microanalysis, 2006, 12, 796-797.	0.4	1
246	Inactivation of NADPH oxidase organizer 1 Results in Severe Imbalance. Current Biology, 2006, 16, 208-213.	3.9	98
247	Heterogeneous uptake and reactivity of formic acid on calcium carbonate particles: a Knudsen cell reactor, FTIR and SEM study. Physical Chemistry Chemical Physics, 2005, 7, 3587.	2.8	80
248	Surface Reactions of Carbon Dioxide at the Adsorbed Waterâ^'Iron Oxide Interface. Journal of Physical Chemistry B, 2005, 109, 12227-12230.	2.6	89
249	Enhanced Photocatalytic Activities of Ag/ZnO Powders Modified by Diblock Copolymer. Advanced Materials Research, 0, 770, 34-37.	0.3	0
250	Water Adsorption on Hydroxyapatite and Struvite as a Function of Relative Humidity: Application of BET and Freundlich Adsorption Models. ACS Earth and Space Chemistry, 0, , .	2.7	8
251	Dynamic Control of Liquid Biomass Digestate Distillation Combined with an Integrated Solar Concentrator Cycle for Sustainable Nitrogen Fertilizer Production. ACS Sustainable Chemistry and Engineering, 0, , .	6.7	5